

Sensitivity analysis for in-cylinder soot-particle size imaging with laser-induced incandescence

E Cenker, G Bruneaux, T Dreier, C Schulz

▶ **To cite this version:**

E Cenker, G Bruneaux, T Dreier, C Schulz. Sensitivity analysis for in-cylinder soot-particle size imaging with laser-induced incandescence. Applied Physics B - Laser and Optics, 2015, 119 (4), pp.745-763. 10.1007/s00340-015-6009-0 . hal-01174701

HAL Id: hal-01174701
https://hal.science/hal-01174701

Submitted on 9 Jul 2015

HAL is a multi-disciplinary open access archive for the deposit and dissemination of scientific research documents, whether they are published or not. The documents may come from teaching and research institutions in France or abroad, or from public or private research centers.

L'archive ouverte pluridisciplinaire **HAL**, est destinée au dépôt et à la diffusion de documents scientifiques de niveau recherche, publiés ou non, émanant des établissements d'enseignement et de recherche français ou étrangers, des laboratoires publics ou privés.

Sensitivity analysis for in-cylinder soot-particle size imaging with laser-induced incandescence

E. Cenker[1,2,3] (✉), G. Bruneaux[1,2], T. Dreier[3], and C. Schulz[3]

[1] IFP Energies Nouvelles, 1 et 4 avenue de Bois-Préau, 92852 Rueil-Malmaison, France
[2] École Centrale Paris, Chatenay-Malabry, France
[3] Institute for Combustion and Gas Dynamics – Reactive Fluids (IVG) and Center for Nanointegration Duisburg-Essen (CENIDE), University of Duisburg-Essen, Duisburg, Germany

✉ emre.cenker@uni-due.de (corresponding author)
gilles.bruneaux@ifpen.fr
thomas.dreier@uni-due.de
christof.schulz@uni-due.de

Abstract

Soot particle sizes can be determined from time-resolved laser-induced incandescence (LII) in point measurements where full signal traces are detected. For instantaneous imaging, strategies are required that must cope with time-gated information and that rely on assumptions on the local boundary conditions. A model-based analysis is performed to identify the dependence of LII particle-size imaging on the assumed boundary conditions such as bath gas temperature, pressure, particle heat-up temperature, accommodation coefficients, and soot morphology. Various laser-fluence regimes and gas pressures are considered. For 60 bar, fluences that lead to particle heat-up temperatures of 3400–3900 K provided the lowest sensitivity on particle-sizing. Effects of laser attenuation are evaluated. A combination of one detection gate starting at the signal peak and the other starting with 5 ns delay was found to provide the highest sensitivity at 60 bar. The optimum gate delays for different pressures are shown. The effects of timing jitter and poly-dispersity are investigated. Systematic errors in pyrometry imaging at 60 bar is evaluated.

Keywords

Laser-induced incandescence; soot particle-size imaging

1. Introduction

In combustion, soot is of major concern because of the stringent regulations of particulate matter emission. Meeting these regulations requires the understanding of formation, growth, aggregation, and oxidation of soot. A quantitative understanding of these processes enables the development of methodologies to limit pollutant emissions and to develop soot prediction models to be used in CFD (computational fluid dynamics) codes [1,2]. Primary particle size and its spatial distribution during the combustion are essential information for the investigation of soot formation and burn out.

Time-resolved laser-induced incandescence (TiRe-LII) emerged as a powerful *in situ* technique for measuring particle sizes. Soot particles are heated via absorption of light from a laser pulse to temperatures well above flame temperature and the subsequent blackbody radiation is recorded during the heat-up and cooling phase. Particle-size information can be obtained from a best-fit comparison of the temporal signal decay and simulations based on the particle's energy and mass balance equations [3–6]. For particle-size measurements, signal traces are usually measured with high time resolution with photomultipliers (PMT). However, this approach is limited to point-wise measurements. The spatial distribution of particle sizes can be revealed only with repeating the measurements at different locations – an approach not possible for rapidly fluctuating situations like those in internal combustion (IC) engines. Will et al. [7–9] developed a strategy for two-dimensional particle sizing where LII signals are acquired at two delay times after the laser pulse with gated intensified cameras and where the particle size is deduced from the local signal ratio. This technique provided particle-size distributions with high spatial resolution for laminar flames at atmospheric pressure [7–10].

In many practical combustion devices, however, soot formation occurs at elevated pressure in time-varying turbulent flames where pressure, temperature, and local gas-phase concentrations have a significant effect on soot formation [11]. In this study, the applicability of time-gated LII particle-size imaging is numerically investigated for engine-relevant conditions. At high pressure, the lifetime of the LII signal is significantly reduced due to enhanced heat exchange of the particles with their environment. Because of this rapid cooling, the normalized LII signal decay profiles for particle classes of different size fall into a very narrow envelope, and curves measured under different conditions become similar to each other. The effects of such convergence on particle-sizing is analyzed.

The influence of the assumed boundary conditions, such as gas-phase temperature, pressure, heat-up temperature, soot morphology, and thermal accommodation coefficient on the simulated LII temporal profiles is quantitatively investigated. The study focuses on 60 bar ambient pressure to mimic Diesel combustion and LIISim [6,12] is used for the simulations. For a sensitivity analysis of the LII signal with respect to boundary conditions that are assumed for data interpretation, a control LII signal is generated for a known particle size and environmental conditions. Subsequently, this simulated signal trace is fitted with a LII model function by systematically changing the assumed values for the relevant boundary conditions within a given range (one by one). The differences between the evaluated sizes and the initial particle size for the control signal show the sensitivity of the particle-size measurement on the respective parameters.

For LII under high-pressure conditions, a known problem is that in poly-disperse soot samples a non-uniform heat-up temperature distribution is reached among the different particle size groups [11,13]. At high pressure, conductive cooling during the nanosecond laser pulse is not negligible which leads to lower heat-up temperatures of the small particles compared to the larger ones. In this present work the resulting variations in heat-up temperature are determined for moderate and high laser fluences for 60 bar and the effect on particle sizing is evaluated. LII diagnostics can also be affected by attenuation of the pump laser [2,14,15]. Laser attenuation causes spatial variations in heat-up temperatures along the laser path. The influence of this effect on particle-size measurements is also evaluated.

For the purpose of potential imaging applications, various detector gating strategies are assessed to maximize the sensitivity of the particle-size evaluation. Various gate widths and delays are convoluted with the simulated time-dependent signals. By determining the variation of the ratio of both gated signals within the range of expected particle sizes, the sensitivity of the gating strategies can be obtained. Previous experiments [2] showed that the gating approach can be significantly affected by timing jitter which was up to ±2 ns. Because of the short signal lifetime at high pressure, such jitter can cause severe changes in the gated signals and their ratio. Effects of such timing jitter are included in the evaluation. The loss in the temporal information compared to the evaluation of full signal traces prevents a detailed analysis of particle-size dispersion. The evaluated particle sizes more represent mono-disperse equivalent mean particle diameters and are inherently biased to the larger sizes. The magnitude of this bias is investigated for soot ensembles with lognormal particle size distribution.

Two-color pyrometry is often used to measure particle heat-up temperatures (related to the effective laser fluence) [13,16,17] along with the LII signal traces. Nevertheless, in two-dimensional measurements at high pressure, the LII signal lifetime is only marginally longer than the gate duration required for signal collection. Therefore, truly instantaneous measurements of peak temperature cannot be achieved because the signal already decays during the detection gate duration and thus, the results are biased to lower temperatures. Like in particle-sizing, laser jitter also influences the results. An accuracy and jitter analysis for two-color pyrometry imaging of heated particles is achieved based on Planck's thermal radiation modeling.

2. Methods

2.1. General Approach

Particle-size measurements with time-resolved LII are based on the fact that, after the initial laser pulse, smaller particles cool down faster than larger ones due to their larger surface-to-volume ratio [18]. In a quantitative approach, assuming that all soot primary particles are spheres, the temperature and size of any known particle size can be modeled for any given time by solving the energy and mass balances. As a consequence, the size of a particle can be evaluated from the temporally-resolved temperature or incandescence signal by using a numerical scheme. In this study, LIISim, developed by Hofmann et al. [6,12] is used for this analysis. The heat exchange mechanisms considered in the LIISim are:

$$\dot{Q}_{abs} = \dot{Q}_{int} + \dot{Q}_{cond} + \dot{Q}_{rad} + \dot{Q}_{evap} \quad (1)$$

where $\dot{Q}_{abs}$ is the energy flux of laser absorption, $\dot{Q}_{int}$ is the rate of change of total internal energy, $\dot{Q}_{cond}$ is the energy flux related to heat conduction, $\dot{Q}_{rad}$ is the heat loss due to radiation, and $\dot{Q}_{evap}$ is the energy flux due to evaporation of material from the surface. The latter term is effective only when the total energy gain due to absorption is sufficient to heat the particle above the vaporization threshold. Once the evaporation starts, soot particles are subjected to a mass loss and the mass of the gas phase increases. This mass balance is described as

$$\frac{dm_{\mathrm{p}}}{dt} = J_{\mathrm{evap}} \qquad (2)$$

with the particle mass m_{p}, the time t, and the mass flux J_{evap}. The underlying physics of all heat- and mass-exchange mechanisms used in LIISim are explained in the literature [6,12] and therefore will not be discussed here. Even though LIISim includes an evaporation sub-model, it should be noted that the current understanding of evaporation is not accurate. Therefore, it is recommended to avoid high laser fluences to keep the soot temperature below the vaporization threshold. For atmospheric conditions, evaporation starts around 3300–3400 K [13] and becomes considerable above 3700 K, however soot evaporation at 60 bar is not exactly known.

LIISim allows choosing between mono- or poly-disperse particles. It is known that soot formation, surface growth, and oxidation are continuous processes and therefore primary soot particles in a flame are poly-disperse which LIISim describes as log-normal distributions. In real systems, primary particles tend to form aggregates [19,20]. A soot particle within an aggregate cools down slower than an isolated single particle because of shielding by surrounding particles. These effects are considered in LIISim as well and the details of poly-dispersion and aggregation can be also found in Refs. [1,6].

For moderate or low laser fluence, which can be simulated by keeping heat-up temperatures below 3500 K, evaporation is negligible and cooling is dominated by heat conduction. Increasing pressure further increases conduction and significantly reduces the LII lifetime [21]. Fig. 1 shows normalized LII signals for various particle sizes at 60 bar. Such a collection of simulated data that forms the basis for subsequent analysis is called a signal “library” in this paper.

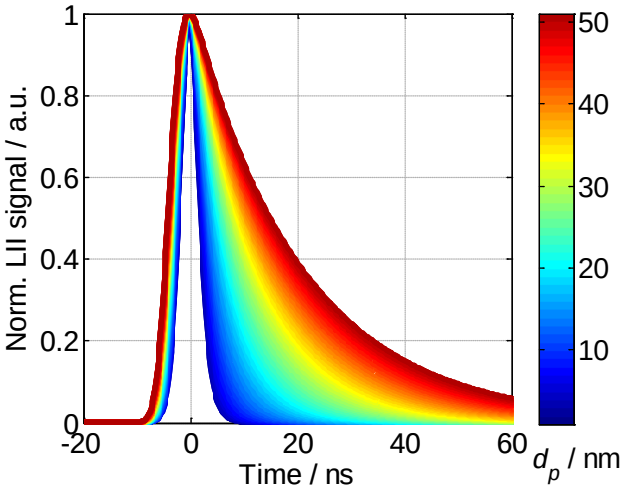


Fig. 1: LII signal "library" showing normalized time-dependent LII-signals for various primary soot particle diameters (d_p) at 60 bar.

In these simulations the particles are assumed to be graphite-like and hence values of material constants associated with graphite are used [22]. For heat conduction the Fuchs approach [23] is chosen in LIISim for high-pressure modeling. Other relevant boundary conditions are given in Tab. 1.

Tab. 1: Boundary conditions for modeling the control signal

LII model input	**Modeled control signal**
Ambient pressure	60 bar
Detection spectral range	410–440 nm
Bath gas temperature	1800 K
Laser fluence at 1064 nm	0.15 J/cm^2
Laser duration (FWHM)	7 ns
$E(m)$	0.4
Aggregate size	50
Thermal accomm. coeff.	0.25

Transmission electron microscope (TEM) [24–26] studies of thermophoretically sampled soot from high-pressure flames show that primary particle sizes typically vary in between 5 and 40 nm. Fig. 1 shows that in this range the LII signal lifetime (time between 100 and 5 % of peak signal) varies from ~6 to ~47 ns. Therefore, when determining particle sizes from LII lifetimes, small uncertainties in data acquisition or modeling can lead to considerable errors. Fig. 1 shows that particle-size-dependent conductive cooling is already relevant during the heat-up phase as each curve has a different shape. In practical applications, nanosecond Nd:YAG lasers are widely preferred in LII soot research for their availability, high power and pulsed operating modes. These lasers have typically Gaussian temporal profiles with a full width at half maximum of 6–8 ns. Particles reach the maximum temperature only after some delay (~7 ns) after start of absorption. Within this period, particles loose energy at different rates depending on their size and therefore they have different signal histories in this phase. As a consequence each particle-size class reaches a different peak temperature [11]. This shows that including the heat-up phase in the simulation of the LII signal is essential in high-pressure LII particle sizing. Effects related to the heat-up phase in high-pressure environments are discussed in section 3.2.

2.2. LII imaging

With the state-of-the-art intensified camera technology, it is not possible for a single detector to provide consecutive images within the typical LII cooling time and multiple detectors (that are in few cases combined into a single “camera”) must be used. The temporal resolution of the collected data depends on the number of imaging detectors. In experiments in stationary flames the temporal LII signal trace can be determined with a single imaging sensor through time-gate sweeping relative to the laser pulses [7,8,10]. This study evaluates a two-camera strategy for instantaneous imaging in turbulent flows.

Both images can be acquired with various delays [7,27] and gate widths [28,29] within the signal decay. Both cameras must capture different temporal information so that the ratio of both signals is a sensitive measure of the decay. For each combination of delays and gate widths, signals and signal ratios can be computed by convoluting the temporal characteristics of the detectors with and the respective LII signal shown in Fig. 1. There is a unique ratio of the two gated signals for each particle size as shown in Fig. 2. The ratio relates the signal in the second gate (delayed) to the first gate and therefore is always below unity. The resulting look-up table is then used for evaluation of the measured data. The example shown in Fig. 2 is based on data for the conditions in Tab. 1 and presents “look-up curves” for laser fluences from 0.05 to 0.15 J/cm^2. These curves are based on evaluated libraries simulated for all fluences with 0.01 J/cm^2 increments. Unless otherwise stated, virtual gates with top-hat (rectangular) temporal profiles of 15 ns are assumed for both gates.

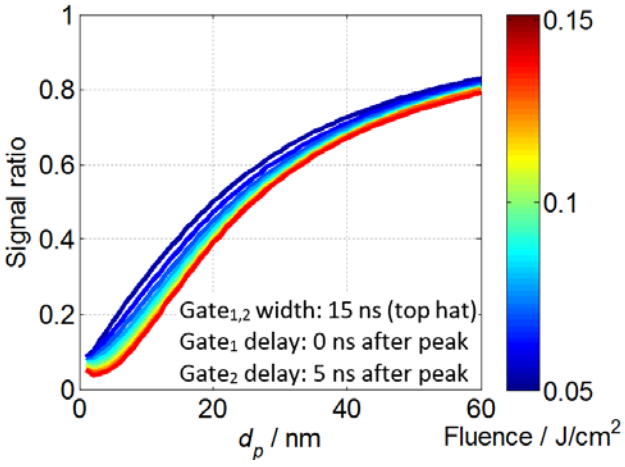


Fig. 2: Look-up table for the particle size as a function of signal ratio created from a modeled library. The influence of the laser fluence is shown for 0.05 to 0.15 J/cm^2 (0.01 J/cm^2 increments).

The comparison of an experimentally-obtained signal ratio image with known laser fluence with this look-up table allows to determine particle sizes for each pixel. It is, however, important, that local conditions are well known. Fig. 2 shows that for a given signal ratio, a variation in the laser fluence by 0.1 J/cm^2 can cause a 60% deviation in particle size. Fig. 2 also shows that for fluences above 0.08 J/cm^2, particles smaller than 4 nm cannot be evaluated because the simulated results are ambiguous.

Crucial for LII particle-size imaging is optimizing the delays of the detector gates. Will et al. [7] showed an optimum timing for high-fluence scenarios at atmospheric conditions that provided the minimum contribution from photoelectron noise to the signal ratio. Mewes and Seitzman [27] reported that both gates must be placed in the temporal section of particle cooling past the end of the laser pulse to provide good size sensitivity. To optimize gate timings, several effects must be considered such as particle-size dispersion, signal-to-noise ratio, LII lifetime, jitter, and detector gate width. For the 60 bar case considered here, weak signals and hence signal-to-noise ratios are the major concern. This strongly restricts the choice of potential gate timings. Fig. 1 shows that the LII signal of a 20 nm diameter particle falls below the 10% of its peak value in less than 20 ns. Therefore, only gates in the vicinity of the signal peak provide sufficient signal. Effects of gate timing are discussed in section 3.4.

3. Results and discussion

3.1. Sensitivity to boundary conditions

A reference LII model function is generated for all subsequent comparisons that is calculated for mono-disperse soot particles with 30 nm diameter with the boundary conditions shown in Tab. 1. Using this signal and the identical boundary conditions as input for the curve-fitting procedure, the original 30 nm size is reproduced. By systematically changing one individual boundary condition (and keeping all others fixed) in the curve-fitting routine, the sensitivity of the system to the respective variable can be determined from the deviation in the evaluated results. Sensitivities of the LII particle-sizing to the thermal accommodation coefficient, bath gas temperature, peak temperature, aggregate size and ambient pressure are shown in Fig. 3. Each plot has two *x*-axes: The axis on the top shows the nominal value of the modified variable whereas the axis on the bottom indicates the relative change of the variable with respect to the control boundary conditions.

The thermal accommodation coefficient, denoted by α_T, describes the efficiency of energy transfer during molecular collision in the heat conduction mechanism. Various values from 0.07 to 1.00 were reported in the literature. A larger value of α_T leads to a more efficient loss of energy to the surrounding atmosphere and, hence, a faster signal decay at the same collision rate [1,30]. α_T is a dimensionless coefficient and depends on temperature as well as on particle morphology [31]. Therefore, it cannot be directly measured in real systems. In this study, the control signal is simulated with a value of 0.25, and various values from 0.1 to 0.4 with 0.01 increments are tested for particle size evaluation. Fig. 3a shows that a too small value of α_T results in smaller evaluated particle sizes because it leads to too slow simulated signal decays. To match the input data, this slow decay is compensated by a small particle size, hence faster decay, by the curve-fitting algorithm. Vice versa, for too large α_T values, too large particle sizes are returned. A 40% inaccuracy in α_T causes as a 20% inaccuracy in the evaluated results.

The bath gas temperature (Fig. 3b) is a physical property of the system. It affects both the radiative and the conductive heat transfer rates and it defines the initial temperature of the soot particles before the laser heat-up. Therefore, the peak temperature of soot and the evaporation rate also depend on the bath gas temperature. To understand how the particle-size evaluation is influenced by incorrect assumptions of the gas temperature, these mechanisms are investigated independently. During laser heating with a constant laser fluence, the peak temperature of the particles increases with increasing gas temperature. This slightly increases the radiative heat flux which remains, however, negligible compared to conductive cooling. For conduction, the bath gas temperature has competing effects. While increasing the gas temperature enhances the thermal conductivity and the heat capacity of air, and thus increases particle air energy transfer, the overall conduction-related heat flux reduces due to a smaller temperature difference ΔT between particle and surrounding gas. Additionally, depending on the laser fluence, the increased bath gas temperature may eventually cause the particle temperature to exceed the evaporation threshold and therefore causes additional energy loss. Fig. 3b shows that with increasing gas temperature at moderate laser fluence, the decrease in heat conduction due to a reduced ΔT is larger than the sum of enhancing effects in the other mechanisms. Therefore, smaller particle sizes are evaluated to compensate the reduced LII signal decay rate when higher gas temperatures are assumed. According to this evaluation, a 20% error in ΔT causes as a 20% error in the evaluated particle sizes.

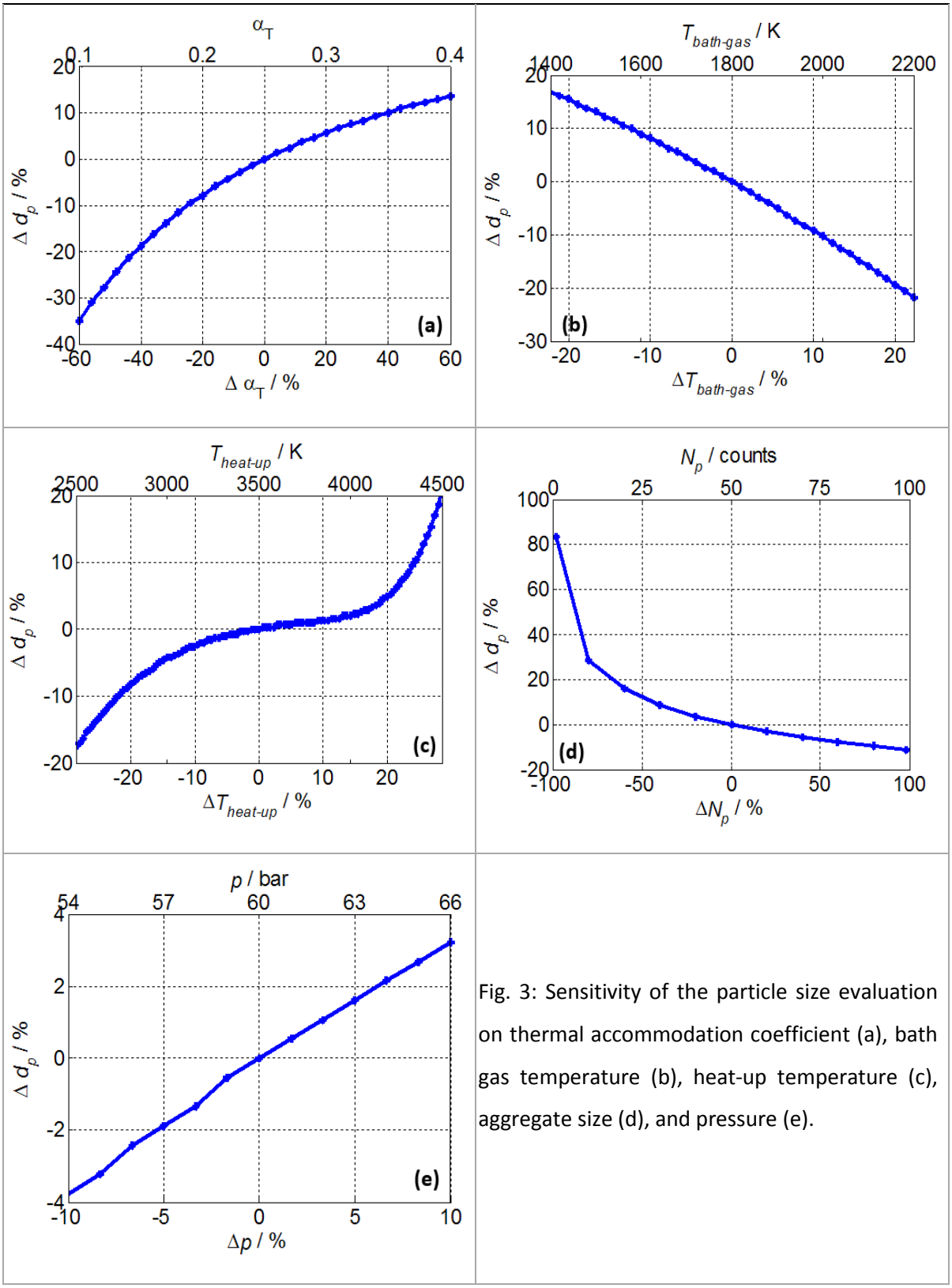


Fig. 3: Sensitivity of the particle size evaluation on thermal accommodation coefficient (a), bath gas temperature (b), heat-up temperature (c), aggregate size (d), and pressure (e).

The particle heat-up temperature (Fig. 3c) reached during the laser pulse depends on the laser fluence chosen for the experiment. As in the case of bath gas temperature, the signal decay and therefore the size evaluation is influenced by the heat-up temperature via radiation, conduction, and evaporation. In all three heat transfer mechanisms, an overestimated heat-up temperature causes faster LII decay that then leads to the prediction of too large particle sizes. The sensitivity of the particle sizing to heat-up temperature is largest in the evaporation regime because the large heat loss encountered with evaporation. Fig. 3c shows that the heat-up temperature has the lowest sensitivity for moderate peak temperatures between 3400 and 3900 K. Tuning the laser fluence to this target temperature range minimizes the uncertainty in size evaluation for the case calculated here at 60 bar.

Soot aggregates can be described as random fractal structures. When modeling LII-signal traces, the laser absorption rate, the change in internal energy and the heat loss due to radiation are not affected by aggregation as long as the individual particles remain in the Rayleigh regime. The signal scales linearly with the number of primary particles within an aggregate, N_p, and hence the mass [12]. However, heat conduction is affected by aggregation. A primary soot particle within an aggregate cools down more slowly than an isolated one because collisions with gas molecules are reduced by the surrounding particles. This phenomenon is known as shielding. Fig. 3d shows that an underestimation of the N_p causes too fast simulated LII decays resulting in an overestimation of particle sizes. The greatest change occurs when switching in LIISim from isolated particles to the aggregate model. N_p, however, is a difficult parameter to measure. The variable range (1–100) investigated here is based on a statistical analysis of TEM measurements of thermophoretically sampled soot obtained from high-pressure combustion processes [19,32]. The ambient pressure is a significant parameter for the shielding-related change in heat flux [12].

The ambient pressure (Fig. 3e) is also a physical property of the system under investigation. In a combustion chamber it is spatially uniform and can be measured by pressure transducers. The pressure affects both conductive cooling and evaporation, while the latter effect is negligible. When the pressure is underestimated, a slower heat exchange, and hence longer signal lifetime is modeled. In such case, the curve-fitting compensates this slower decay by returning smaller particles. The deviation in the particle size was not greater than ±4% for an error of ±10% in pressure. Nevertheless, the pressure and the signal lifetime have a logarithmic relation (cf. section 3.4 and Fig. 12). Around 60 bar, the influence

of pressure on particle-sizing can be marginal whereas at pressures lower than 10 bar, small deviations can lead to large discrepancies.

Besides its direct effect, the pressure influences the sensitivity of the particle-sizing to the other experiment and modeling parameters. To determine the effect of pressure on the influence of the bath gas temperature, the analysis shown in Fig. 3b was repeated at pressures from 1 to 80 bar. All the other modeling parameters were kept constant. Fig. 4a shows that, as pressure increases, the sensitivity of the evaluation to the input data reduces. When the bath gas temperature is assumed 20% lower than the actual temperature, the error on the evaluated size is around 30% at atmospheric pressure whereas this error reduces below 15% at pressures above 60 bar. The same analysis is repeated for the heat-up temperature and shown in Fig. 4b. At atmospheric conditions, a 20% higher heat-up temperature can cause errors above 60%, whereas the same variation causes only 5% error at pressures above 40 bar. This reduction in the sensitivity can be attributed to the fact that at higher pressures the normalized LII signal decay traces of different particle sizes fall into narrower envelopes and curves resulting from different environmental conditions become closer.

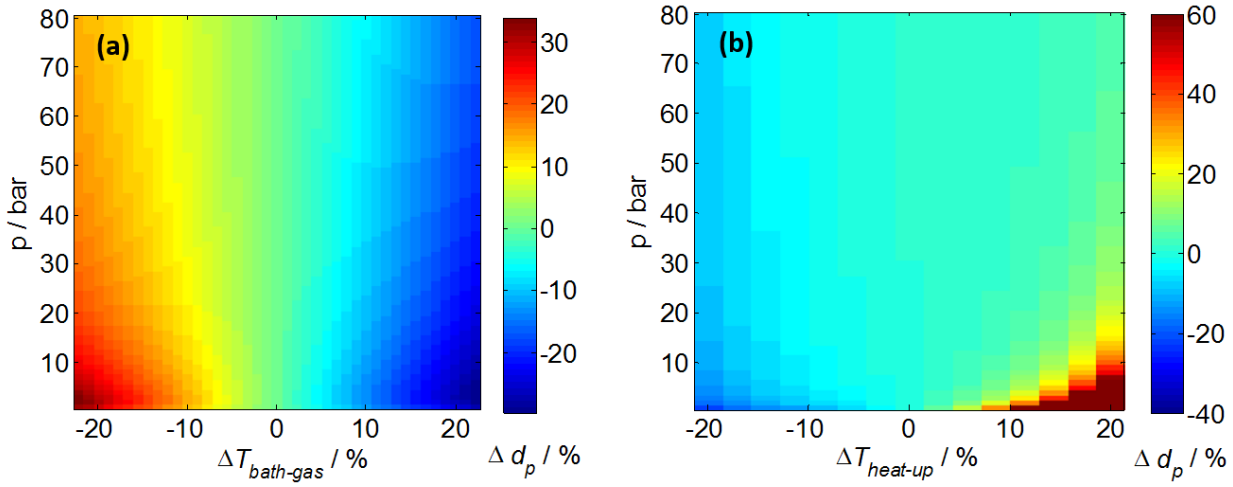


Fig. 4: Sensitivity of particle-sizing to the bath-gas temperature (a) and heat-up temperature (b) at various pressures

3.2. Particle-size dependent heat-up temperature

Within the Rayleigh regime, $\pi d_{\mathrm{p}}/\lambda_{\mathrm{ex}} < 0.3$, (with λ_{ex} the laser wavelength) the energy absorbed by a particle depends on its volume [6]. Independent of the particle size, the same energy density is reached

and all particles in a poly-disperse ensemble should reach a uniform heat-up temperature as long as no energy losses occur during heat-up. These losses, however, can be significant at high pressure. Recent studies [11,13] showed that the particle-size dependent energy loss during heat-up causes temperature differences among the different particle size groups in the ensemble because small particles loose energy faster than larger particles. To quantify these deviations at 60 bar, simulations were performed for the evaporating and non-evaporating regime for particle diameters from 2 to 50 nm at conditions given in Tab. 1.

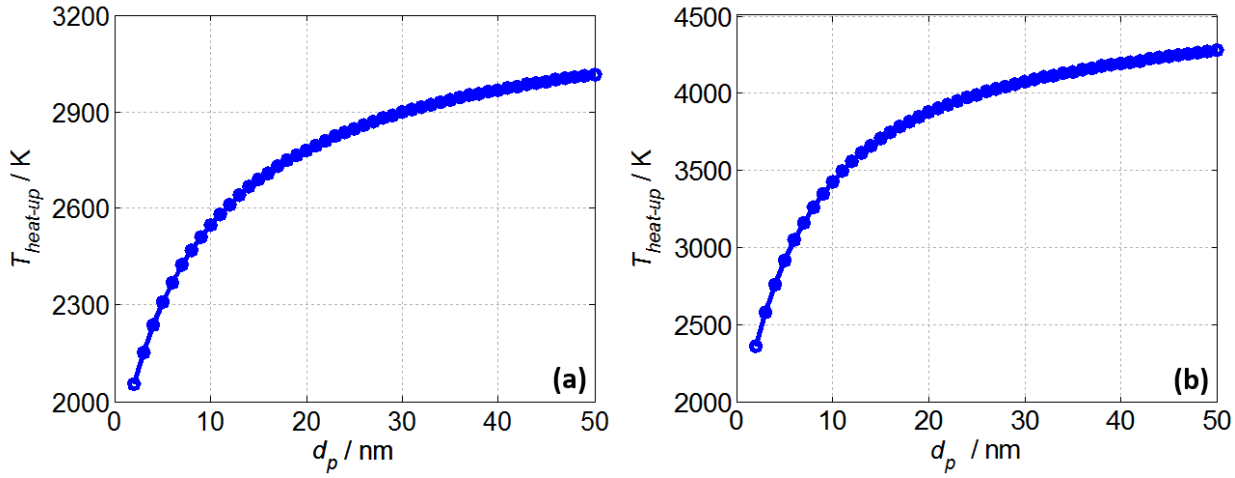


Fig. 5: Particle-size dependent peak temperatures, $T_{\mathrm{heat-up}}$; (a) non-evaporating regime (0.08 J/cm^2), (b) evaporating regime (0.2 J/cm^2).

For low laser fluences (Fig. 5a) the peak temperature difference between the 10 and 40 nm particles is ~400 K while for the high-fluence regime (Fig. 5b) it is above 600 K. As shown in section 3.1, such deviations in heat-up temperature can have dramatic effects on particle-sizing. This effect also limits the reliability of the pyrometric determination of heat-up temperatures that are used for two-color LII measurements where the modeling of the laser absorption is omitted and the measured temperature is used as an input for the simulation [11,12,21,33,34]. In particle-size measurements that include heat-up modeling, the variation in peak temperatures is automatically considered because a unique peak temperature, hence a peak LII signal, is calculated for each trace with the net energy gain. Nevertheless, uncertainty still remains for poly-disperse soot where the acquired experimental signal trace (or signal ratio in particle-size imaging) consists of radiation from various particle size groups. Uncertainties related to poly-dispersion are discussed in section 3.6.

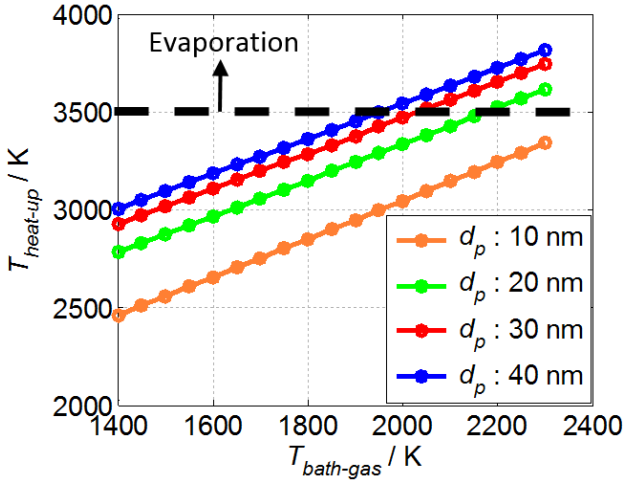


Fig. 6: Dependence of particle heat-up temperatures on bath-gas temperatures for various particle sizes.

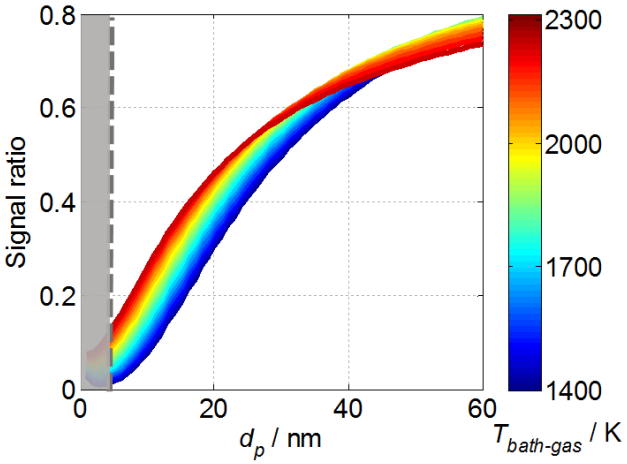


Fig. 7: Look-up table of d_p vs. signal ratio for gas temperatures, $T_{\mathrm{bath-gas}}$, between 1400 and 2300 K with a laser fluence of 0.15 J/cm^2.

The relation between particle size and peak temperature can also influence evaporation. For a given laser fluence, depending on the bath gas temperature, the peak temperature of small particles may remain below the evaporation threshold whereas larger particles may start to evaporate. The dependence of the peak temperature to the bath gas temperature for different diameters are presented in Fig. 6. The simulations are performed with the parameters shown in Tab. 1. 10-nm particles cannot reach evaporation regardless of the bath gas temperature in the investigated temperature range. On the other hand, 40-nm particles reach the evaporation threshold for gas temperatures above 2000 K eventually causing an accelerated heat loss for larger particles and affecting the LII signal trace after the

peak, thus the sensitivity of the particle-sizing on the various parameters changes for different size groups. This influence on the cooling phase can be seen in Fig. 7, where the look-up table of the particle size vs. signal ratio is given for gas temperatures between 1400 and 2300 K with 100 K increments and for particle sizes between 1 and 60 nm. The remaining parameters are those from Tab. 1. For the analysis, a delay of 5 ns between the two detection gates is considered. In the particle size domain smaller than 35 nm, for a given signal ratio, larger particle sizes are determined at smaller gas temperatures. Nevertheless, low and high gas temperature curves show different characteristics: For large particles at high gas temperatures the ratio of the two time-gated signals falls below the simulations for lower gas temperature. This is related to a combined effect of the onset of evaporation and particle-size dependent peak temperatures. Results for particle sizes below 4 nm are shaded because they are beyond the limit of particle-sizing with the conventional signal simulation provided by LIISim. To avoid the complications of the particle-size dependence on the peak temperature, Charwath et al. [11] proposed faster short-pulse laser heating to temporally separate from particle cooling. However, Michelsen [35] reported that rapid heating with conventional picosecond lasers brings new complications to the particle-sizing and requires new modeling approaches. Unconventional laser sources with pulse durations of ~1 ns would potentially be a good compromise, but they are not readily available and have not yet been explored for LII.

3.3. Effects of laser attenuation

Sooting high-pressure flames provide strongly absorbing environments that can affect laser-based diagnostics. Attenuation of the laser beam causes a spatial variation in laser fluence along the beam propagation direction. Strategies that rely on ratioing of two signals often reduce or avoid the dependence of the signal of interest on laser fluence. While this works with strategies where the signal linearly depends on the laser fluence, such as two-color laser-induced fluorescence methods [36], it is not applicable to LII because the fluence affects the signal and its decay characteristics in multiple ways. The magnitude of laser attenuation depends on the optical density of the soot cloud, KL, which is linearly proportional to the soot volume fraction along the laser path. A comprehensive explanation of laser attenuation in sooty environments is given in Refs. [14,37]. Laser attenuation eventually causes a spatial variation in the heat-up temperatures of the particles within the imaged area. Fig. 8 shows the dependence of the peak temperature on laser fluence. Simulations were performed for Tab. 1 conditions. The variation of $T_{\text{heat-up}}$ with particle size at the low-fluence limit and the slopes observed for

the investigated particle sizes are due to the dependence of the energy-loss rates during the heat-up on the particle size (cf. section 3.2). The influence of laser fluence on the peak temperature is more significant in moderate or low-fluence LII. In the high-fluence regime (>0.25 J/cm^2) the sensitivity decreases due to the very strong heat loss through evaporation.

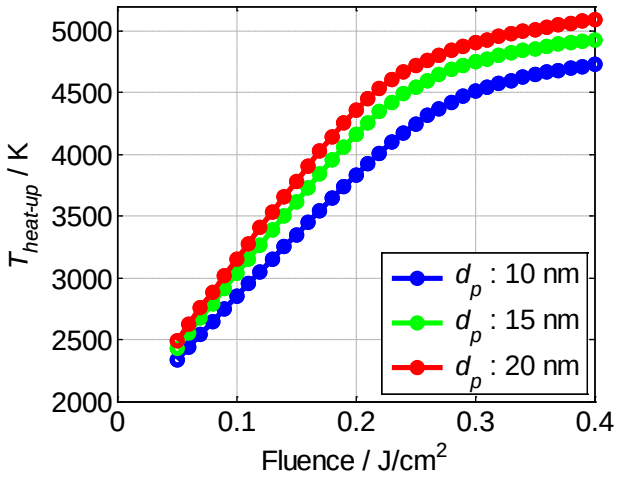


Fig. 8: Particle peak-temperature as a function of laser fluence for 10, 15, and 20 nm particle diameter.

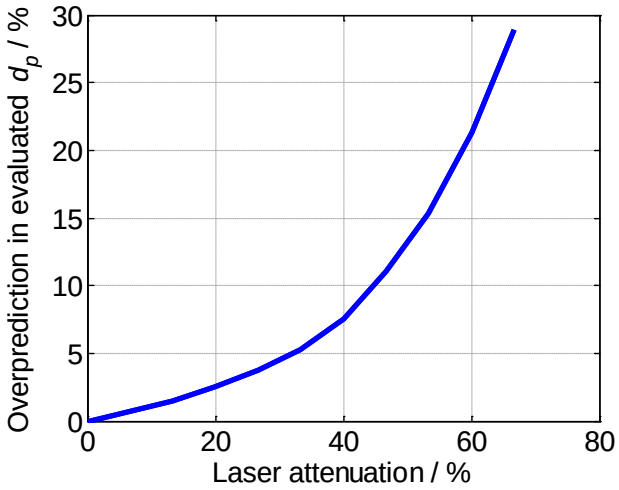


Fig. 9: Error in the evaluated particle size as a function of laser attenuation (conditions of Tab. 1).

Fig. 9 shows the effect of laser attenuation on the evaluated particle size for 30 nm particles for Tab. 1 conditions. When laser attenuation is not taken into account, the heat-up simulation calculates too high peak temperatures resulting in too fast signal decays. To compensate, the curve-fitting routine yields too large particles. To eliminate the attenuation-related uncertainty, the effective laser fluence at each

pixel should be known. Although it is relatively easy to measure the total attenuation, it is not trivial to measure the fluence gradient along the soot environment. To achieve this, temperature gradients of heated soot particles can be measured via two-color pyrometry imaging and resulting temperature can be used to calculate the effective laser fluences. Nevertheless, the gas temperature and particle size variations also affect the peak temperature as previously described which reduces the precision of the fluence measurements (For two-color pyrometry imaging of heated particles, cf. section 3.7).

3.4. Gating strategies

Optimizing timing and width of the two detector gates is crucial to optimize the sensitivity of the signal ratio to particle size and to maintain good signal-to-noise ratios. Both images must be acquired during the signal lifetime and record information at different points in time. Three gating strategies are investigated in this section:

Reference strategy

In order to understand the effect of the gate width on the determination of particle-sizes, the signal-ratio method was investigated analytically. In an experiment where heat conduction is the dominant heat transfer mechanism, the LII signal of a monodisperse class of particles, either isolated or aggregated, decays nearly exponentially [38]. With this assumption, the approximated signals collected by two gates with identical width can be calculated as

$$I_1 = \int_0^{\Delta t} e^{-t/\tau} dt = -\frac{1}{\tau}\left(e^{-\Delta t/\tau} - 1\right) \quad (3)$$

$$I_2 = \int_{\delta}^{\delta+\Delta t} e^{-t/\tau} dt = -\frac{1}{\tau} e^{-\delta/\tau}\left(e^{-\Delta t/\tau} - 1\right) \quad (4)$$

Where Δt is the gate width, τ is the lifetime and δ is the delay for the beginning of the second gate with respect to the signal peak. The ratio *R* of the two signals,

$$R = \frac{I_2}{I_1} = e^{-\delta/\tau}, \quad (5)$$

is independent on the gate width. Nevertheless, to minimize the detection of background signal (e.g., flame luminosity), the gates should be as short as possible. On the other hand, the camera gate should be long enough to collect sufficient signal to minimize the signal-to-noise ratio. In recent experiments, 15 ns were identified as the shortest gate that yields sufficiently strong signal at conditions comparable

to Tab. 1, and therefore, this value is taken as the base gate width in this study. Nevertheless, depending on the camera, the optical setup, the laser fluence, the laser sheet thickness, and the soot volume fraction, optimum gate widths may change.

To optimize the delay δ between the detection gates for highest sensitivity to particle size, further calculations were performed. The best sensitivity is given in the case with the strongest variation of the signal ratio vs. particle size. Therefore, the dynamic range, *DR*, of a signal-ratio curve was evaluated over the entire range of particle sizes. Based on Eq. 5, *DR* can be calculated for a given δ as

$$DR = R(\tau_L) - R(\tau_S) = \exp{}^{-\delta}/_{\tau_L} - \exp{}^{-\delta}/_{\tau_S}, \quad (6)$$

where the subscripts *L* and *S* represent the largest and smallest particles in the measurement domain, respectively. *DR* is 0 at $\delta = 0$ and it increases with increasing δ, since τ_L is larger than τ_S. However, as δ goes to infinity, *DR* converges to 0. Hence, *DR* reaches a maximum at a certain δ (δ^*, optimum delay) and this value can be calculated from the zero value of the derivative of *DR* with respect to δ:

$$\frac{dDR}{d\delta} = -\frac{1}{\tau_L}\exp{}^{-\delta^*}/_{\tau_L} + \frac{1}{\tau_S}\exp{}^{-\delta^*}/_{\tau_S} = 0 \quad (7)$$

From Eq. 7, the optimum delay for the second gate is

$$\delta^* = (\ln(\tau_L) - \ln(\tau_S))/\left(\frac{1}{\tau_S} - \frac{1}{\tau_L}\right) \quad (8)$$

Eq. 8 indicates that the optimum delay yielding the highest sensitivity is solely related to the lifetime of the LII signal which depends on various parameters and needs to be simulated. Therefore, to determine δ^* for the conditions shown in Tab. 1, a model-based analysis was performed. For the first analysis the starting time of the first gate was fixed to the peak signal to confine the input data to the cooling part of the LII signal where the simple exponential approximation is valid (cf. Eq. 3 and 4). Delaying the first gate leads to a loss in signal and the signal contribution from the smallest particles will be reduced. Advancing of the first gate with respect to the peak signal will be considered later. This analysis is targeted to identify the optimum timing of the second gate that provides the highest sensitivity to particle sizing and that provides sufficient signal. Therefore, the second gate is swept along the modeled data library with a delay from 1 to 20 ns with respect to the first gate. A look-up curve that relates the signal ratio to particle size and thus indicates the sensitivity of the measurement strategy is created for each delay δ (cf. Fig. 10a).

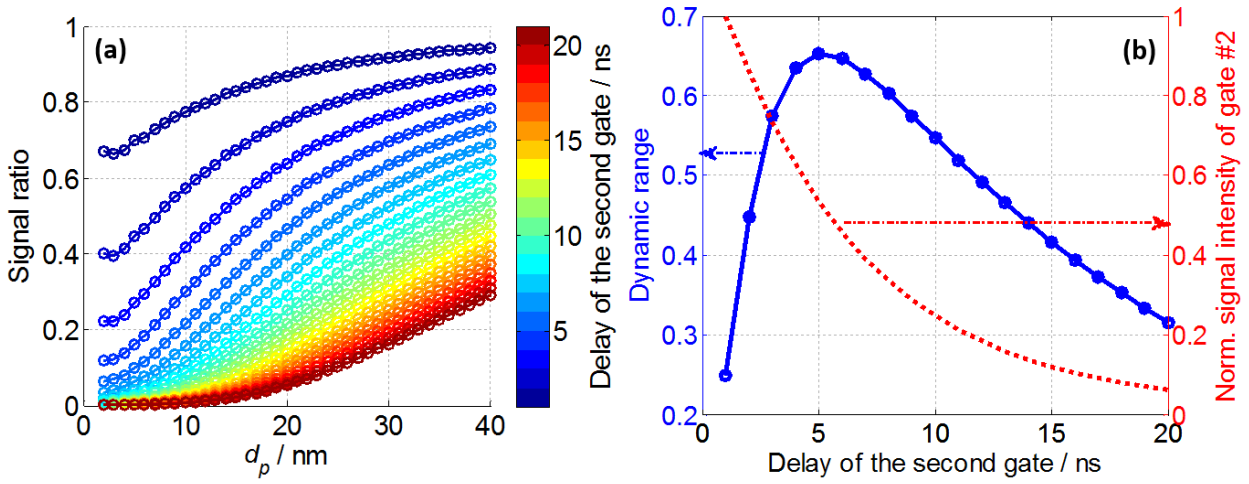


Fig. 10: (a) Look-up curves for various delays of the second gate δ with fixed 15 ns gate width and the first gate starting at the signal peak, (b) dynamic range of signal ratios for particles from 4 to 40 nm diameter for different delay scenarios (solid blue curve) and the integrated signal intensities with the second gate for an average expected particle diameter of 20 nm (dotted red curve). The signal-intensity curve is normalized to the signal at δ = 1 ns.

The dynamic range *DR* of each look-up curve was calculated for the particle size-range expected for engine-like combustion (4–40 nm). The solid blue curve in Fig. 10b shows that a delay of 5 ns yields the largest dynamic range, (signal ratio varies in the 0.06–0.73 range between 4–40 nm) hence the highest sensitivity is reached for Tab. 1 conditions. Remembering the 15 ns width for both gates, this results in a 10-ns overlap of both gates. The reason of the reduction in sensitivity at longer delays is that small particles cool down to the ambient temperature within the delay time and thus, the second gate cannot capture any signal from these particles anymore. This can be seen through the decreasing slopes of the look-up curves for increasing delay in the particle domain smaller than 10 nm diameter in Fig. 10a. In contrast, when the delay is too short, both images capture too similar information. Therefore, the ratio of the images converges to 1 and the sensitivity is reduced.

While searching for the maximum dynamic range *DR*, it is also important to consider the signal intensity in the delayed gate. Depending on the experimental parameters (see above), too long delays lead to insufficiently weak signal and thus increased signal-to-noise ratios. The red dotted curve in Fig. 10b shows how the signal intensity declines relative to a 1-ns delay scenario for a particle diameter of 20 nm (expected average particle size). At a delay of 5 ns, which was calculated as the delay yielding the largest

dynamic range, the theoretical signal intensity in the second gate is 53% compared to the case with the minimum delay (1 ns). Concerns, however, are related to the nominal signal intensity (photon counts) and the actual signal-to-noise ratio. The nominal signal changes from system to system, and it is therefore not easy to speculate a universal relative threshold that still provides acceptable signal. Ideally, the signal strength in both channels should be comparable. In this study we decided that second-gate signals lower than 5% of first-gate signals are considered too low. The sections of the signal ratio curves (in Fig. 10a) that are below 0.05 are therefore not taken into account.

The influence of the ambient pressure on δ^* is investigated by evaluating the above-mentioned maximum points on dynamic range curves which were created with unique libraries for different pressures as shown in Fig. 11. Optimum delay δ^* is plotted on a log-scale. For each library the remaining conditions from Tab. 1 were used. When the pressure increases, the lifetime of the LII signal and therefore, δ^* decreases as shown in Eq. 8.

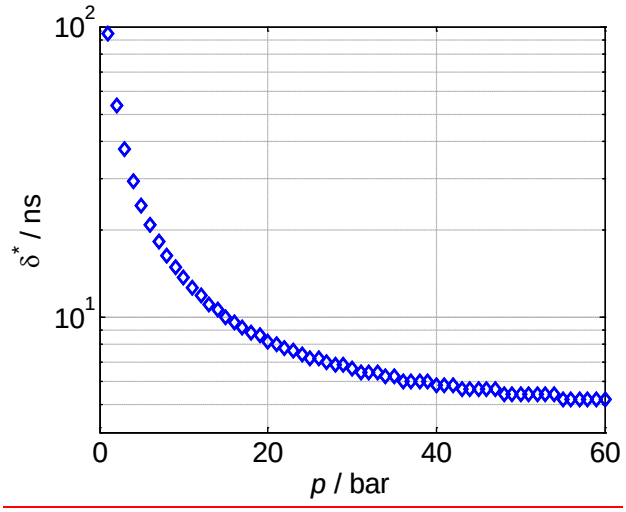


Fig. 11: Optimum delay δ^* for the second gate at various ambient pressures (The first gate starts at signal peak)

It can be also seen that the rate of change in δ^* reduces with increasing pressure. In conduction cooling, the heat flux from particle to the bath gas is proportional to the pressure. Thus the lifetime is inversely proportional to the pressure. The relation between signal lifetime and pressure for soot aggregates with 30-nm diameter particles at Tab. 1 conditions is shown in Fig. 12. After the first few ten bar, the lifetime

shows an asymptotic behavior and does not change significantly with increasing pressure. Therefore, from 20–60 bar, δ^* changes only by 3 ns.

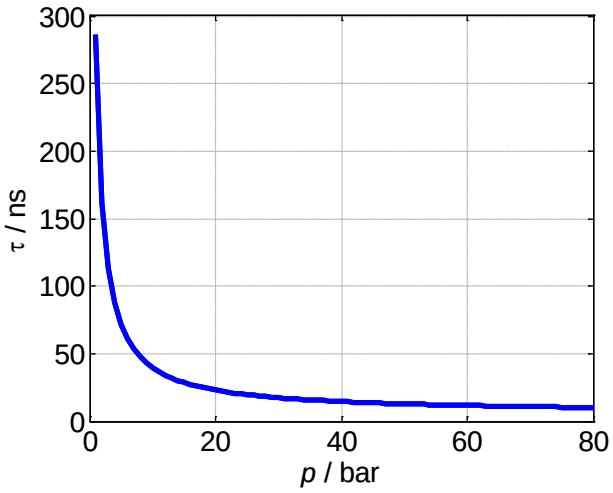


Fig. 12: LII-signal lifetime as a function of pressure.

Gate-advancing strategy

In the previous strategy the second gate always provides much weaker signal than the first gate. Shifting the second gate to early times in contrast reduces the sensitivity because of a large overlap of the detected signals. An alternative strategy is advancing the first gate to start before the signal peak is reached. This allows to increase the signal in both gates with a limited effect on the sensitivity. Up to a certain advancing time the sensitivity slightly reduces but with further increasing of advancing time, the sensitivity recovers and exceeds its initial value. Obviously, it does not make sense to advance the first gate to times before the onset of the laser pulse; therefore, the discussion is limited to advancing times between –7 and 0 ns before the signal peak.

The theoretical analysis of these cases requires model libraries that include the simulation of the heat-up phase (cf. section 3.2). In contrast to the LII-signal decay, the slope of the LII signal on the heat-up side is almost identical for all particle sizes. The relative contribution of signal from small particles therefore increases when advancing the gate. Fig. 13a shows the variations in signal intensity of the first gate (blue curves) and the second gate (red curves) at the respective δ^* ~~(to be explained)~~ as a function of advancing times for 4-nm (dashed curves) and 40-nm (solid curves) particles. Each curve is normalized to the respective value without advancing the gate. Advancing the first gate increases the signal in the first gate (up to 70 and 21% for 4 and 40 nm particles, respectively). For each position of the first gate,

the second gate is swept up to a delay δ of 20 ns relative to the first gate. For each position of the first gate, there is a unique "best" δ^* derived from the maximum of the dynamic-range curves in Fig. 13b. The relative signal increase in the second gate with respect to the original case is substantial (up to 1480% and 52% for 4 and 40 nm particles respectively). Advancing the first gate up to –4 ns slightly reduces the sensitivity of particle sizing (maximum dynamic range is reduced by 5%). However from –4 to –7 ns, the sensitivity starts to increase (maximum dynamic range reaches 8% more of the original case at –7 ns advancement).

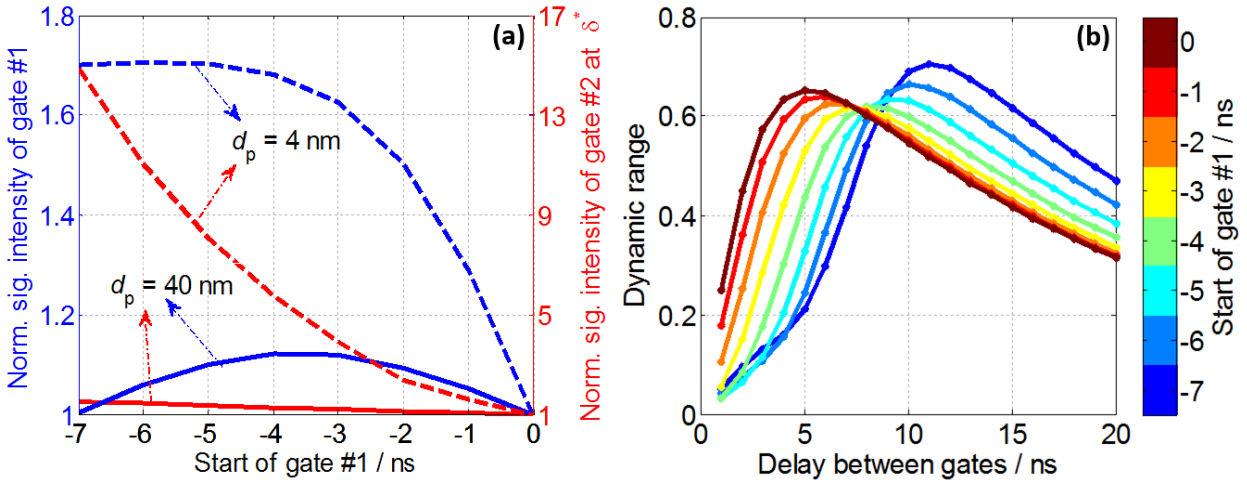


Fig. 13: (a) Integrated signal intensities with both gates at various advancing times for two different particle sizes. Each curve is normalized to the respective value without advancing the gate. (b) Dynamic range *DR* of the signal ratio *R* for particles from 4 to 40 nm diameter with advanced first gate.

With increasing time advancing of the first gate, the relative increase in signal intensity in the second gate (at δ^*) is substantially larger than in the first gate for small particles. Nevertheless for larger particles, the signal intensity increase in both gates is comparable. Therefore, the signal ratio increases more for small particles than for large ones and the look-up curves become flatter (the dynamic range decreases). This continuous up to –4 ns. At an advancing time greater than –4 ns, the integrated signal intensity in the first gate starts to decrease for larger particles with increasing time advancing whereas it keeps rising in the second gate (cf. Fig. 13a) due to shifting towards the peak. This leads to a rapid increase in the signal ratio at the large particle classes. In this time range the increasing signal ratio at the small particle classes remains marginal relative to the increase in large classes. As a result, the dynamic range, and hence, the sensitivity of particle sizing, increases slightly from –4 to –7 ns (cf. Fig.

13b). The analysis shows that advancing of the first gate to the start of laser heating (–7 ns) and a delay of 11 ns between the two gates is the optimal gate strategy. This strategy enhances the signal-to-noise ratio as the signal intensity in both channels increases. It also increases the sensitivity of particle-sizing by 8% with respect to the original case without gate advancement.

Asymmetric gating strategy

A further enhancement of the signal-ratio based particle-sizing is possible by using asymmetric gate widths. For the delayed gate, the original 15 ns may be too short to collect signal leading to poor signal-to-noise ratios. Starting with the optimum strategy mentioned above (first gate at –7 ns, 11-ns delay between both gates), the width of the second gate is extended from 15 to 55 ns with 1 ns increments. For each gate width, a look-up curve is created (Fig. 14). The extension of the second gate has no impact on the signal ratio of the small particle classes because the original 15 ns duration was sufficient to capture all the signal information of these small particles. For larger particles, however, the signal increases when increasing the gate width. This leads to an increase of the signal ratio for the large particle classes, hence an increase of the particle-size sensitivity. After a certain gate width, the second-gate signal becomes stronger than the first-gate signal and the ratio *R* exceeds unity.

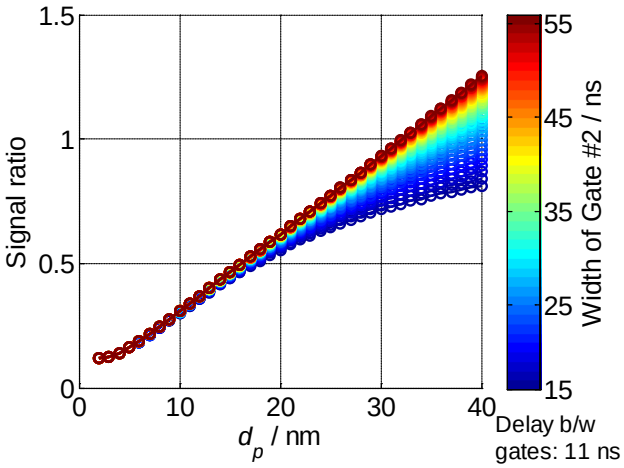


Fig. 14: Look-up curves for asymmetric gate widths. The width of the second gate is extended from 15 to 55 ns with 1 ns increments. The first gate is fixed to –7 ns and has a constant 15 ns width. The second gate is fixed to 11 ns after the first gate. The sensitivity increases with increasing gate width.

By extending the second gate from 15 to 35 ns, the dynamic range and hence the sensitivity increase by 50%. Fig. 14 shows that the further effects when extending the gate from 35 to 55 ns (from yellow to

dark red) are marginal. In contrary, such long gates might negatively impact the accuracy because of the increasing contribution of background (e.g. flame luminosity).

After all, the ultimate strategy can be defined as: The first gate should be advanced to the start of particle heating (–7 ns in this study). The width of the second gate should be about twice as long as the first gate (here: first gate: 15 ns, second gate: 35 ns) and it should start 11 ns after the first one. As previously explained, all these nominal timing values (given here for the conditions given in Tab. 1) depend on the experimental conditions.

3.5. Effects of timing jitter

In practical experiments jitter might occur between the laser pulse and the gated signal detection. Due to the short LII signal lifetime at high pressure, even a small jitter can cause considerable errors. For the analysis, the 5 ns delay between the two detection gates is considered fixed and it is assumed that the laser is the source of the jitter. The effect of shifting the laser pulse relative to the detection event by –4 ns up to +4 ns was simulated with 0.5 ns increments (positive values: Laser fires later than expected). For each time-shift a new look-up curve is created and for a given “true” particle size of 30 nm an “evaluated” particle size is determined by using the original look-up curve without jitter.

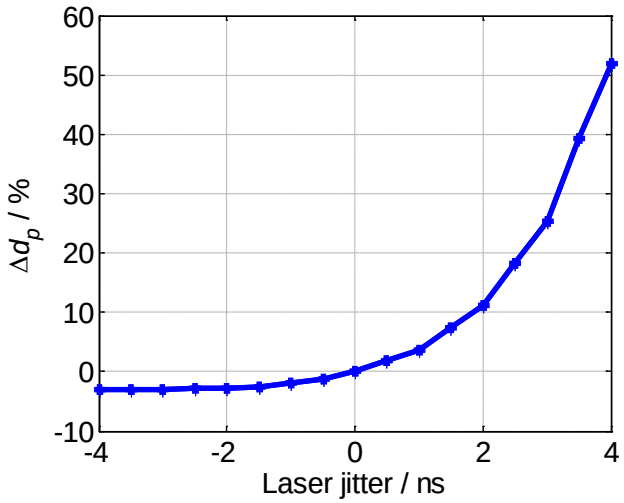


Fig. 15: Effect of laser timing jitter with respect to camera gates on the evaluated particle size; the delay between the two gates is fixed.

Fig. 15 shows the strongly asymmetric effect. With a positive jitter, the first camera gate starts before the signal peak leading to a signal loss relative to the second gate, thus increasing the gate #2/gate #1

ratio resulting in an overprediction of the particle size. A +2 ns jitter leads to an overprediction by 10%. With a negative jitter both detection gates are shifted into the range of decaying signal. In this case, smaller signal ratios and an underpredicted particle size are determined. Compared to the positive jitter, the discrepancies associated with the negative jitter are marginal. This is because the jitter has a similar effect on both gates and shifting along the nearly exponential decay; the gate ratio is better preserved. Nevertheless, this analysis does not consider the influence of the reduced signal-to-noise ratio when the jitter reduces the overall signal intensities. With negative laser jitter, the LII signal can decrease drastically in both channels.

If jitter cannot be fully avoided for any reason, to minimize jitter-related uncertainties a temporally-resolved acquisition working simultaneously with the imaging system can be implemented. By reading the actual laser and camera timings, identical delays can be taken into account when creating the look-up curves. By this means, measured and simulated signal ratios will be related to the same LII signal theoretically. Such evaluation algorithm will be effective only if the heat-up modeling is included in the signal library. When the absorption part of the LII signal is missing, the gate convolution on the model library with positive laser jitter encounters zero signal on the left side of the peak signal, whereas, on the experiment side, cameras still collect strong signal during the heat-up phase.

3.6. Influence of poly-dispersity

Heat conduction is the dominant cooling mechanism of soot particles at high pressure heated below the evaporation temperature. Along this cooling, the decay rate remains unchanged for a mono-disperse sample and therefore it can be approximated by a single-exponential decay. In a poly-disperse ensemble, each size group has a unique LII signal decay rate. During a measurement, the signals of these different groups superimpose resulting in a deviation of the acquired signal from the single-exponential decay. The relative contribution of each size group is linearly proportional to its relative soot volume fraction. In a particle size evaluation with the conventional time-resolved entire signal fitting approach, additional information about the different size groups can be extracted by using a pre-assumed distribution [13]. However, it should be noted that it is generally challenging to fit poly-disperse distributions to LII signals due to the fitting problem being ill-posed [39,40]. Instead, the signals can be fitted with mono-disperse model signals and therefore the evaluated result for the signal acquired from the poly-disperse soot ensemble is an averaged mono-disperse equivalent mean particle size. Comparisons with TEM measurements showed that the mono-disperse equivalent size is always larger

than the count median diameter of the poly-disperse TEM distribution, due to the fact that fitting with mono-disperse assumption biases the average results towards larger sizes [39]. The reason of this bias can be attributed to the dominance of the contribution of the large particles to the collected signal due to their longer and stronger incandescence as stated above. At high pressure, the particle-size dependent peak temperature (cf., section 3.2) causes additional bias towards the larger sizes since their contribution increases with temperature to the fourth power. The difference in the magnitude of the signal can be seen in Fig. 16 with LII curves modeled for the conditions in Tab. 1.

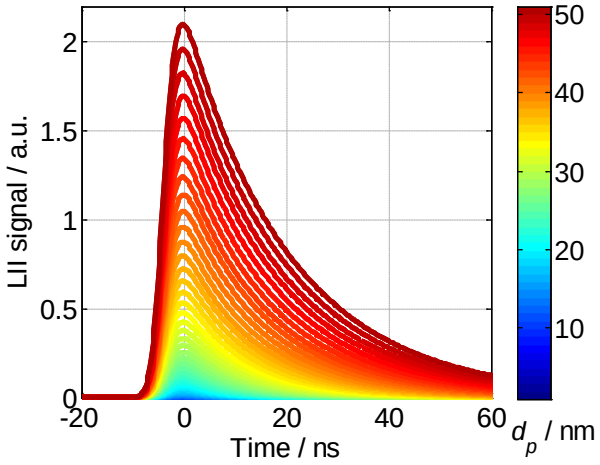


Fig. 16: LII signal traces for particles of different size. The magnitude of the signal is proportional to the third power of the particle diameter and fourth power of its temperature.

When sizing particles using the ratio of two gated signals, decay rates are not directly accessible and the signal interpretation results from the comparison with pre-calculated look-up tables. These are based on signal libraries that are created from simulations for the behavior of mono-disperse soot. The evaluation of the signal acquired from poly-disperse soot again yields averaged mono-disperse equivalent mean particle sizes. In this section, we investigate the magnitude of this bias towards larger sizes based on the signal-ratio method for the conditions shown in Tab. 1. Fig. 17a shows lognormal soot particle size distribution functions (related to the respective particle volume) for three different counter mean diameters, d_{cmd} = 10, 20 and 30 nm, but with identical geometric width, $\sigma_g = 1.4$, and each data point on the curve represents the probability density of a 1 nm-wide bin. Using these distribution functions and the particle-size-dependent signals from Fig. 16, LII signal traces for the respective polydisperse ensembles were calculated. After applying the convolution with the gate timings shown in section 3.4, an averaged mono-disperse equivalent mean particle size was evaluated from the look-up tables in Fig.

2 and shown as vertical dash-dotted lines. By using the same methodology, in Fig. 17b, the bias towards larger sizes are shown for particle size distribution functions with σ_g = 1.2, 1.4, and 1.6 with identical d_{cmd} at 20 nm.

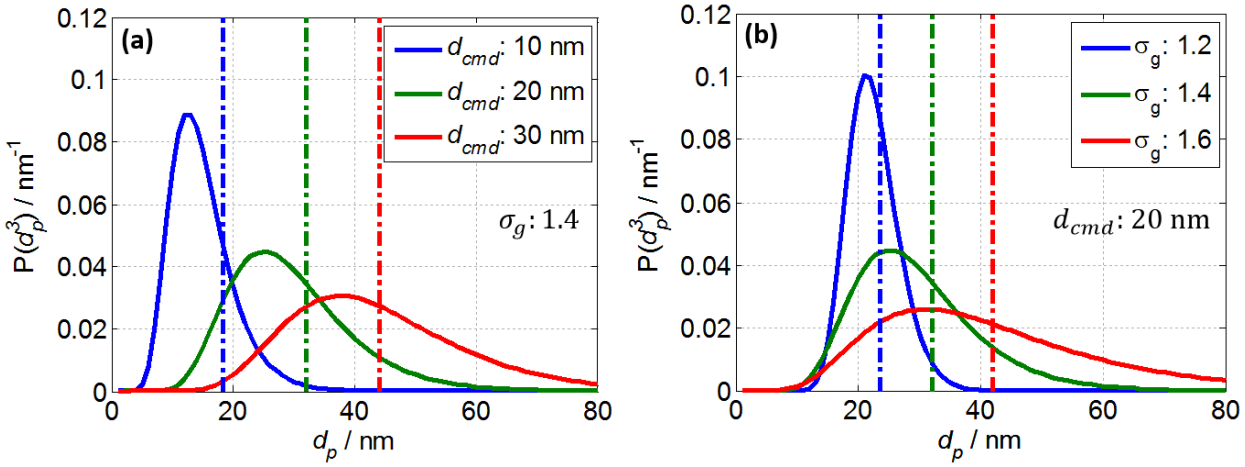


Fig. 17: (a) Lognormal distribution functions of particle sizes (related to soot particle volume) for three count mean diameters; fixed geometric width at 1.4, (b) lognormal distribution functions of soot particle sizes for three different geometric widths; with d_{cmd} = 20 nm. Vertical dash-dotted lines show the mono-disperse particle size evaluated by the signal ratio method for the LII signal input of soot ensembles having the distribution function with the respective color.

In all cases, the evaluated mono-disperse equivalent mean particle sizes are larger than the mean of the input distribution. In a lognormal distribution, the weight of larger particles in the probability density function increases with the increasing lognormal mean. This can be seen in Fig. 17a with the extending tail of the distribution for larger d_{cmd}. As a result, the bias in the evaluated particle-size increases because the relative contribution of the small particles to the ensemble signal is lower than the larger ones. Fig. 17b shows that the bias is getting smaller for narrower distributions. Nevertheless, it should be noted that the magnitude of the bias in the signal-ratio method directly depends to the delay for the second gate as shown in section 3.4. As the delay increases, the contribution of smaller particles in the second gate further decreases and the bias increases.

To investigate the additional bias at high pressures due to the particle-size dependent peak temperature, seven different signal libraries were created with ambient pressures from 1 to 60 bar with Tab. 1 conditions. From each library, a poly-disperse signal was created by using the lognormal

distribution with d_{cmd} = 15 nm and $\sigma_g = 1.5$. For each pressure the optimum delay for the second gate shown in Fig. 11 was used and the mono-disperse equivalent mean particle size with the signal ratio were calculated, shown in Fig. 18. The temperature difference between small and large particles increases with increasing ambient pressure. Therefore, at higher pressure the relative contribution of the smaller particles in the ensemble poly-disperse signal reduces causing the bias of the mono-disperse equivalent mean particle size to increase.

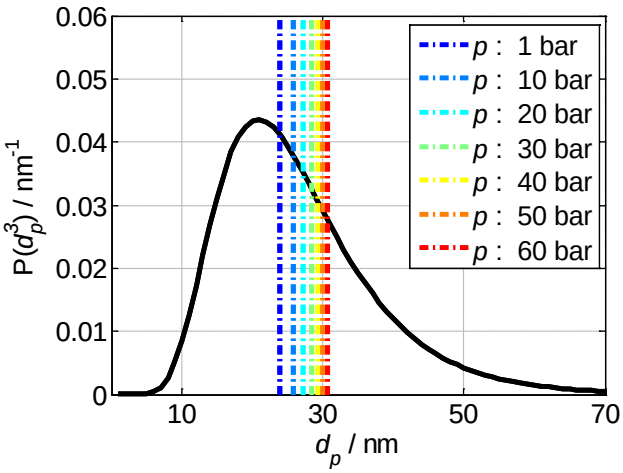


Fig. 18: Bias of the mono-disperse equivalent mean particle size (vertical dash-dotted lines) towards larger particles at different pressures. The distribution function of soot particle volume is a lognormal with d_{cmd} = 15 nm and $\sigma_g = 1.5$.

3.7. Gating effects on two-color pyrometry

In cases where the laser fluence changes locally, e.g., because of laser attenuation, it is advantageous to measure the spatial distribution of heat-up temperatures which allows to consider the local conditions during data evaluation. Two-color pyrometry imaging of the particle temperature during laser heating can provide the required information. At high pressure, however, a compromise must be found: The short lifetime of the incandescence signal requires an as short as possible detection exactly at the peak to avoid biasing of the measurement towards lower temperatures. On the other hand, sufficient signal must be detected for low-noise measurements, which prevents the use of short gates. Furthermore, jitter of the laser timing relative to the detector gates could strongly affect the measurement when the gates are very short. To analyze the influence of the gate lengths and the measured apparent peak temperature, time-resolved temperature information is extracted from the control LII signal with 30 nm

particle size with the boundary conditions given in Tab. 1. The expected signal intensities within two detection bands centered at 425±15 and 676±14.5 nm are calculated using Planck's equation [41] (cf. Fig. 19: a).

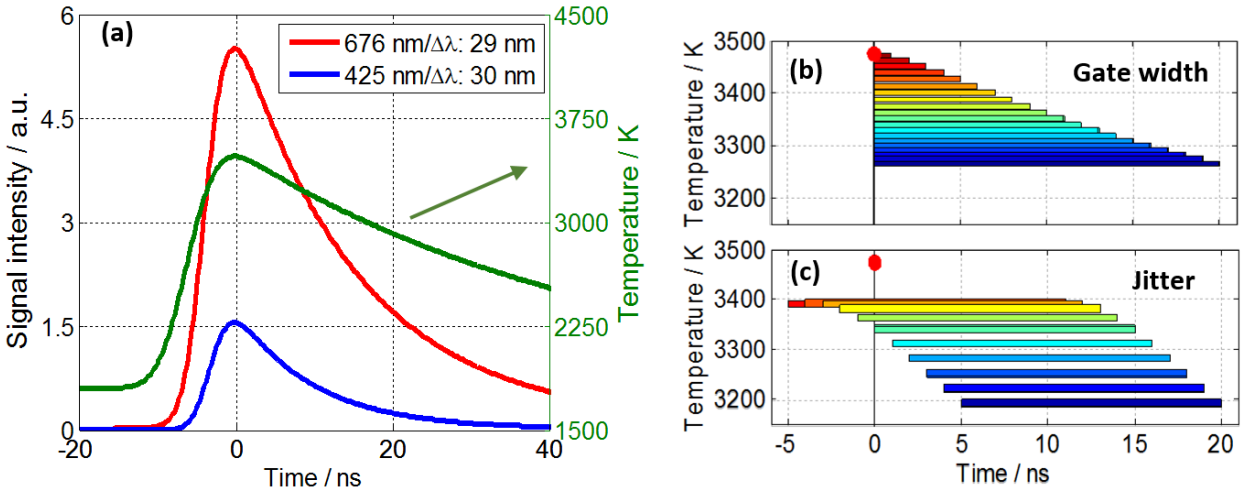


Fig. 19: (a) Time-dependent temperature and thermal emission at 425±15 and 676±14.5 nm calculated for the respective temperature, (b) evaluated apparent temperature for gate widths from 1 to 20 ns, the instantaneous peak temperature is shown with the red dot, (c) evaluated apparent temperature with a fixed 15 ns gate width for jitter from –5 to +5 ns.

To investigate the effect of the time-averaging within realistic camera gates, the calculated thermal emission for the two detection bands is convoluted with gate width from 1 to 20 ns (starting at the signal maximum). The resulting signal ratio is then evaluated based on Planck's law. Fig. 19: b shows the evaluated apparent temperatures on the *y*-axis for each gate width. The red dot shows the instantaneous peak temperature. As the gate width increases, the apparent peak temperature reduces. For a 15-ns gate, the evaluated temperature is underpredicted by roughly 200 K. Fig. 19c shows the effect of laser jitter up to ±5 ns for a gate width of 15 ns. Each bar shows a different jitter scenario and the actual timings can be read on the *x*-axis. If the gates start at a point before the signal peak, the apparent temperature is closer to the actual temperature. In a case where detection starts after the peak, the particles may already have lost some part of their energy and therefore, the calculated temperature can be substantially lower. To minimize the jitter-related uncertainty in an experiment, the gating timing can be set to a couple of nanoseconds before the signal peak so that the temperature

measurement will be less sensitive to timing. This will also reduce the bias of the method towards lower temperature.

4. Conclusions

The applicability of laser-induced incandescence particle-size for high-pressure conditions (such as Diesel combustion) was studied based on a detailed numerical analysis. At high pressure the LII-signal lifetime is short because of efficient conductive cooling of the laser-heated particles. Various gating strategies were compared. To deduce the primary particle size from LII imaging, a look-up table method based on the ratio of two pre-calculated time-gated signals was used. This method was evaluated by applying the data evaluation strategy to simulated signal traces where various parameters were modified systematically. This allows to assess quantitatively the sensitivity of the particle-size determination to the assumed boundary conditions, such as bath-gas temperature, pressure, heat-up temperature, aggregate size, and thermal accommodation coefficients. By systematically changing a single boundary condition at a time, the LII signal trace was simulated via LIISim, convoluted with the characteristics of the detection gates and an apparent particle size was determined from the resulting simulated signal ratio from the look-up table. The evaluated differences between the resulting apparent sizes and the initial particle size provided information about the sensitivity of the method to the respective variable.

It was observed that at elevated pressures there is a substantial difference between the decay rate of isolated soot and aggregated soot. However once the aggregation is considered, the impact of the aggregate size is marginal. The bath-gas temperature has a multifaceted effect on particle-sizing through conductive cooling and the level of the resulting heat-up temperature. It was identified that the particle-size evaluation has the lowest sensitivity to the uncertainties of heat-up temperatures between 3400–3900 K. The sensitivity analysis for bath-gas temperature and heat-up temperature were performed for 1–60 bar and it is observed that for elevated pressures the sensitivity of the LII evaluation to the boundary conditions is strongly reduced. This is attributed to the fact that at higher pressures the normalized LII signal traces of different particle sizes fall into a narrower envelope and curves with different conditions become more similar.

The dependence of the heat-up temperature on the particle size at high pressure is well known. The discrepancy between particles with 10 and 40 nm diameter at 60 bar was calculated as high as 400 K for

a moderate laser fluence. To reduce the uncertainties in particle-sizing arising from this effect, the heat-up phase should be included in the simulation rather than imposing a single peak temperature value (such as derived from two-color LII).

In soot clouds with significant optical density, laser attenuation may cause additional non-uniformity in the spatial distribution of the heat-up temperatures. In a measurement with moderate laser fluence, an attenuation up to 20% causes an error on the particle size less than 3%. For stronger attenuation, however, the error increases. Spatial variation in laser fluence can be measured by soot pyrometry imaging and effective laser fluences can be evaluated from heat-up temperatures.

To find an optimum gating strategy, time-resolved model signals were convoluted with varying gate widths or at varying delays. In the first attempt both gates are confined to the cooling part of the LII signal, and to maximize the signal intensity, the first gate is fixed to the time of maximum signal. It is analytically shown that for monodisperse soot ensembles there is an optimum delay for the second detection gate. This optimum delay depends on the signal lifetime and therefore depends on pressure. In the second attempt the sensitivity of particle-sizing is boosted up to 8% by advancing the first gate to the starting point of the laser-heating and by positioning the second gate to the respective optimum delay. This strategy also provides a significant enhancement to signal-to-noise ratio, yet it is possible only if heat-up modeling is included in the simulations. In the third attempt an extension of the second gate width is added. It is found that a second gate width as two times long as the first one yields an additional 50% increase in the sensitivity along with an additional increase in the signal-to-noise ratio. In a measurement where the signal lifetime and gate widths are short, timing jitter can influence the evaluated results strongly. The effects of timing jitter for particle-sizing and heat-up temperature measurements were shown.

Particle-size imaging based on time-gated signal ratios is inherently a mono-disperse evaluation technique since the necessary information for a more detailed analysis is lost during the convolution and gate delay. The mono-disperse equivalent mean particle size is always biased towards larger sizes. The reason of this bias is due to the dominance of the large particles' contribution to the collected signal due to their longer and stronger incandescence. At high-pressure applications the particle-size dependent peak temperature may cause additional bias towards the larger sizes. These biases are evaluated for different pressures and distributions.

Similar optimum gating strategies were assessed for two-color pyrometry imaging. It is shown that measured heat-up temperatures with such method are biased to lower temperature. At 60 bar, a bias of 200 K was calculated for a particle with 30 nm diameter.

Acknowledgements

The authors thank for Hubert Baya Toda at IFPEN for his help in analytical calculations of gating strategies.

References

[1] C. Schulz, B.F. Kock, M. Hofmann, H.A. Michelsen, S. Will, B. Bougie, R. Suntz, G.J. Smallwood, Appl. Phys. B 83 (2006) 333–354.

[2] E. Cenker, G. Bruneaux, L.M. Pickett, C. Schulz, SAE Int. J. Engines 6 (2013) 352–365.

[3] H.A. Michelsen, F. Liu, B.F. Kock, H. Bladh, A. Boiarciuc, M. Charwath, T. Dreier, R. Hadef, M. Hofmann, J. Reimann, S. Will, P.-E. Bengtsson, H. Bockhorn, F. Foucher, K.-P. Geigle, C. Mounaïm-Rousselle, C. Schulz, R. Stirn, B. Tribalet, R. Suntz, Appl. Phys. B 87 (2007) 503–521.

[4] R. Ryser, T. Gerber, T. Dreier, Combust. Flame 156 (2009) 120–129.

[5] T. Dreier, B. Bougie, N. Dam, T. Gerber, Appl. Phys. B 83 (2006) 403–411.

[6] M. Hofmann, B.F. Kock, C. Schulz, in:, Eur. Combust. Meet., *Chania (Greece), 2007*.

[7] S. Will, S. Schraml, A. Leipertz, Proc. Combust. Inst. 26 (1996) 2277–2284.

[8] S. Will, S. Schraml, A. Leipertz, Opt. Lett. 20 (1995) 2342–2344.

[9] S. Will, S. Schraml, K. Bader, A. Leipertz, Appl. Opt. 37 (1998) 5647–5658.

[10] B.C. Connelly, *Quantitative Characterization of Steady and Time-Varying, Sooting, Laminar Diffusion Flames Using Optical Techniques*, PhD thesis, Yale University, 2009.

[11] M. Charwath, R. Suntz, H. Bockhorn, Appl. Phys. B 104 (2011) 427–438.

[12] M. Hofmann, B.F. Kock, T. Dreier, H. Jander, C. Schulz, Appl. Phys. B 90 (2007) 629–639.

[13] F. Liu, B.J. Stagg, D.R. Snelling, G.J. Smallwood, Int. J. Heat Mass Transf. 49 (2006) 777–788.

[14] L.M. Pickett, D.L. Siebers, Int. J. Engine Res. 7 (2006) 103–130.

[15] L. Francqueville, G. Bruneaux, B. Thirouard, SAE Int. J. Fuels 3 (2010) 163–182.

[16] B. Menkiel, A. Donkerbroek, R. Uitz, R. Cracknell, L. Ganippa, Combust. Flame 159 (2012) 2985–2998.

[17] B.M. Crosland, M.R. Johnson, K.A. Thomson, Appl. Phys. B 102 (2011) 173–183.

[18] L.A. Melton, Appl. Opt. 23 (1984) 2201–2208.

[19] T. Yamaguchi, K. Kondo, H. Nishigai, S. Takano, T. Aizawa, SAE Int. J. Fuels Lubr. 5 (2012) 316–328.

[20] D. Witkowski, K. Kondo, G. Vishwanathan, D. Rothamer, Combust. Flame 160 (2013) 1129–1141.

[21] M. Hofmann, W.G. Bessler, C. Schulz, H. Jander, Appl. Opt. 42 (2003) 2052–2062.

[22] J. Johnsson, H. Bladh, P.-E. Bengtsson, Appl. Phys. B 99 (2010) 817–823.

[23] N.A. Fuchs, Geofis. Pura E Appl. 56 (1963) 185–193.

[24] S. Kook, R. Zhang, K. Szeto, L.M. Pickett, SAE Int. J. Fuels Lubr. 6 (2013) 80–97.

[25] K. Kondo, T. Aizawa, S. Kook, L.M. Pickett, SAE Tech. Pap. (2013) 2013–01–0908.

[26] T. Aizawa, H. Nishigai, K. Kondo, T. Yamaguchi, J.-G. Nerva, C. Genzale, S. Kook, L.M. Pickett, SAE Int. J. Fuels Lubr. 5 (2012) 665–673.

[27] B. Mewes, J.M. Seitzman, Appl. Opt. 36 (1997) 709–717.

[28] B.B. Collier, M.J. McShane, Anal. Chem. 84 (2012) 4725–31.

[29] A. Ehn, O. Johansson, A. Arvidsson, M. Aldén, J. Bood, Opt. Express 20 (2012) 3043–56.

[30] B.F. Kock, B. Tribalet, C. Schulz, P. Roth, Combust. Flame 147 (2006) 79–92.

[31] S. Maffi, S.D. Iuliis, F. Cignoli, G. Zizak, Appl. Phys. B 104 (2011) 357–366.

[32] S. Kook, L.M. Pickett, Proc. Combust. Inst. 33 (2011) 2911–2918.

[33] R. Ryser, T. Gerber, T. Dreier, Combust. Flame 156 (2009) 120–129.

[34] B. Menkiel, A. Donkerbroek, R. Uitz, R. Cracknell, L. Ganippa, Combust. Flame 159 (2012) 2985–2998.

[35] H.A. Michelsen, Appl. Phys. B 83 (2006) 443–448.

[36] S. Faust, G. Tea, T. Dreier, C. Schulz, Appl. Phys. B 110 (2012) 81–93.

[37] M.Y. Choi, K.A. Jensen, Combust. Flame 112 (1998) 485–491.

[38] S. Dankers, A. Leipertz, Appl. Opt. 43 (2004) 3726–3731.

[39] H. Bladh, J. Johnsson, N.-E. Olofsson, A. Bohlin, P.-E. Bengtsson, Proc. Combust. Inst. 33 (2011) 641–648.

[40] K.J. Daun, B.J. Stagg, F. Liu, G.J. Smallwood, D.R. Snelling, Appl. Phys. B 87 (2007) 363–372.

[41] D.R. Snelling, F. Liu, G.J. Smallwood, O. Gulder, Combust. Flame 136 (2004) 180–190.